ELSEVIER

S0032-3861(96)00846-4

Polymer Vol. 38 No. 13, pp. 3269–3278, 1997

0032-3861/97/$17.00 + 0.00

Phase properties in relation to mesogen length in chiral side-chain polysiloxanes

M. Svensson and B. Helgee*
Department of Polymer Technology, Chalmers University of Technology, S-412 96 Göteborg, Sweden

and K. Skarp, G. Andersson and D. Hermann
Department of Physics, Chalmers University of Technology, S-412 96 Göteborg, Sweden
(Received 22 April 1996; revised 29 July 1996)

The synthesis of a series of side-chain liquid crystalline siloxane copolymers is reported, and comparative studies of physical properties of members of the series with different side-chain length have been attempted. All the five members show smectic C* and smectic A phases. Measurements of ferroelectricity, relaxation times and electroclinic properties have been carried out, aiming at finding structure–property relationships for the longer side-chain members. A relationship between electroclinic coefficient and side-chain length was also found. © 1997 Elsevier Science Ltd.

(Keywords: ferroelectric; liquid crystal; side-chain polymer; synthesis; electro-optic switching; polarization electroclinic)

INTRODUCTION

Systematic variation of molecular structure combined with determination of key physical properties is a cornerstone for establishing structure–property relationships in liquid crystals. In the field of low molar mass liquid crystals, such research has a rather long tradition, which has resulted in deeper understanding of some aspects of liquid crystal properties. In particular, the optical and dielectric, and also the elastic properties of nematic liquids can now be correlated to molecular structure in some detail, while a molecular theory for the viscosity parameters of these liquids is still not available. In the area of smectic liquid crystals, the discovery of ferroelectric liquid crystals by Meyer *et al.*[1] in 1974 has opened a new field for structure–property research. In 1982, it was shown possible to incorporate chiral smectic mesogens in side-chain polymers, thus producing ferroelectric smectic polymers[2]. Further studies have shown that these novel polymer systems possess a wide variety of unusual physical properties. Via careful design of the chemical structure of the mesogenic side-chain of the polymers, properties like ferroelectricity[3,4], antiferroelectricity[5,6], pyroelectricity[7,8], piezoelectricity[9,10] and non-linear optical properties[11] have been successfully incorporated in side-chain liquid crystalline polymers. By crosslinking the main-chain polymer it has also been possible to prepare liquid crystalline elastomers which can be oriented by magnetic or electrical fields, or by applying a mechanical stress on the sample[12].

In the field of smectic liquid crystalline side-chain polymers, a few studies have been made concerning the relationship between chemical structure and physical properties [see reviews in refs 13 and 14], but compared to the situation in low molar mass liquid crystals, very little is known in detail for the polymeric systems. Important factors for systematic studies include for instance main-chain side-chain interactions, effects of changes of the chemical structure on the phase behaviour and the phase properties such as the spontaneous polarization of ferroelectric phases.

In the present paper the synthesis and physical properties of a series of side-chain liquid crystalline siloxane copolymers are reported. Previously, we reported electrooptical measurements[15] and non-linear optical properties[16] on two members of the series.

The aim of this study is to obtain correlations between phase behaviour (transition temperatures, ferroelectric and electroclinic properties), and the length of the side-chain. The polymer system consists of a polysiloxane copolymer functionalized with a side-chain based on hydroxy-biphenylcarboxylic acid and R-3-(4-hydroxy-3-nitrophenyl)-2-chloropropionic acid ester attached to the polymer via a C_{11}-spacer. All the polymers show S_C^* phases. The width of the smectic A phase increases with decreasing length of the terminal alkyl ester.

EXPERIMENTAL

Synthetic procedure

Materials and reagents were of commercial grade quality and used without further purification unless otherwise noted. Dry toluene and methylene chloride were obtained by passing the solvents through a bed of aluminium oxide (ICN Alumina N-Super I). Poly(dimethyl-siloxane-*co*-hydrogenmethylsiloxane) and the hydrosilylation catalyst dicyclopentadienylplatinum(II) dichloride were obtained from Wacker Chemie AG.

* To whom correspondence should be addressed

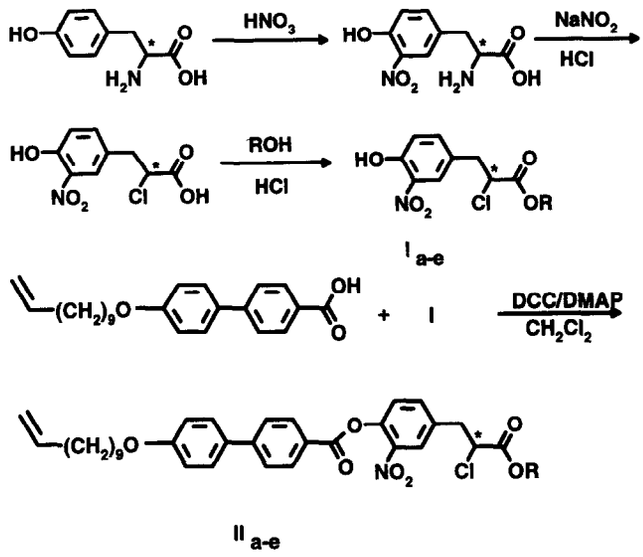

Scheme 1 Synthesis of side-chain mesogen

*R(+)-2-Chloro-3-(3-nitro-4-hydroxyphenyl) propionic acid butyl ester (***Id***).* The synthesis of **Id** was carried out from L(−)tyrosine via nitration[17], diazotization[18] and esterification (*Scheme 1*) without extensive purification of the intermediate products. L(−)Tyrosine, 0.1 mol (18.1 g) was suspended in 85 ml of water and placed on an ice-bath. 30 ml of conc. nitric acid was added gently with stirring. After 1 h the flask was covered with plastic foil and placed in the refrigerator overnight. The red mixture was filtered and the isolated product was reprecipitated from 6 M hydrochloric acid cooled down to 0–5°C and diazotized with 0.1 mol (6.3 g) sodium nitrite in 20 ml of water. The reaction mixture was extracted with ether, dried over magnesium sulfate and evaporated until dry. 2 g of the crude product was esterified in 10 ml butanol using hydrogen chloride gas as catalyst. Excess alcohol was evaporated and the residue was purified on a silica column using petrol ether/ethyl acetate 3/1 as an eluent. The butyl ester forms a yellow oil pure according to t.l.c. and ^{1}H n.m.r. $[\alpha]_D^{20} = +3.07°$ (chloroform). ^{1}H n.m.r.: $\delta = 0.9\ t$ 3H, $\delta = 1.32\ m$ 2H, $\delta = 1.6\ m$ 2H, $\delta = 3.18\ q$ 1H, $\delta = 3.34\ q$ 1H, $\delta = 4.15\ m$ 2H, $\delta = 4.4\ q$ 1H, $\delta = 7.1\ d$ 1H, $\delta = 7.45\ dd$ 1H, $\delta = 7.97\ d$ 1H, $\delta = 10.55\ s$ 0.5H. N.m.r. spectra of intermediate products were in accordance with their respective structure.

The other corresponding esters **Ia**, **b**, **c**, and **e** were prepared in accordance with the procedure of the butyl ester and their characteristics are given below.

*R(−)-2-Chloro-3-(3-nitro-4-hydroxyphenyl) propionic acid methyl ester (***Ia***).* $[\alpha]_D^{20} = -0.77°$ (chloroform). ^{1}H n.m.r.: $\delta = 3.18\ q$ 1H, $\delta = 3.34\ q$ 1H, $\delta = 3.8\ s$ 3H, $\delta = 4.4\ q$ 1H, $\delta = 7.1\ d$ 1H, $\delta = 7.45\ dd$ 1H, $\delta = 7.97\ d$ 1H, $\delta = 10.55\ s$ 0.5 H.

*R(+)-2-Chloro-3-(3-nitro-4-hydroxyphenyl) propionic acid ethyl ester (***Ib***).* $[\alpha]_D^{20} = +2.26°$ (chloroform). ^{1}H n.m.r.: $\delta = 1.3\ t$ 3H, $\delta = 3.18\ q$ 1H, $\delta = 3.34\ q$ 1H, $\delta = 4.2\ m$ 2H, $\delta = 4.4\ q$ 1H, $\delta = 7.12\ d$ 1H, $\delta = 7.48\ dd$ 1H, $\delta = 7.97\ d$ 1H, $\delta = 10.55\ s$ 0.5 H.

*R(+)-2-Chloro-3-(3-nitro-4-hydroxyphenyl) propionic acid propyl ester (***Ic***).* $[\alpha]_D^{20} = +2.36°$ (chloroform). ^{1}H n.m.r.: $\delta = 0.9\ t$ 3H, $\delta = 1.65\ m$ 2H, $\delta = 3.18\ q$ 1H, $\delta = 3.34\ q$ 1H, $\delta = 4.2\ m$ 2H, $\delta = 4.4\ q$ 1H, $\delta = 7.12\ d$ 1H, $\delta = 7.46\ dd$ 1H, $\delta = 7.97\ d$ 1H, $\delta = 10.55\ s$ 0.5 H.

*R(+)-2-Chloro-3-(3-nitro-4-hydroxyphenyl) propionic acid hexyl ester (***Ie***).* $[\alpha]_D^{20} = +3.14°$ (chloroform). ^{1}H n.m.r.: $\delta = 0.9\ t$ 3H, $\delta = 1.29\ m$ 6H, $\delta = 1.6\ m$ 2H, $\delta = 3.18\ q$ 1H, $\delta = 3.34\ q$ 1H, $\delta = 4.15\ m$ 2H, $\delta = 4.4\ q$ 1H, $\delta = 7.1\ d$ 1H, $\delta = 7.47\ dd$ 1H, $\delta = 7.98\ d$ 1H, $\delta = 10.52\ s$ 1H.

4′-Hydroxy-biphenyl-4-carboxylic acid was synthesized in accordance with the method of Percec *et al.*[19].

4′-(10-Undecenyloxy)-biphenyl-4-carboxylic acid. To a hot mixture of 34 mmol (7.3 g) of VI and potassium hydroxide, 86%, (4.4 g) in ethanol (1.0 l) and water (100 ml), undecenyl bromide 68 mmol was added. The reaction mixture was refluxed for 12 h and the ester was hydrolysed by adding a 10% solution of potassium hydroxide in 70% ethanol and refluxing for 2 h. The product was recrystallized from acetic acid and ethanol. Yield 7.9 g (65%). ^{1}H n.m.r.: $\delta = 0.76$–$1.02\ m$ 13H, $\delta = 1.3\ m$ 2H, $\delta = 1.54\ m$ 2H, $\delta = 3.5\ t$ 2H, $\delta = 4.45\ m$ 2H, $\delta = 5.3\ m$ 1H, $\delta = 6.48\ d$ 2H, $\delta = 7.08\ d$ 2H, $\delta = 7.12\ d$ 2H, $\delta = 7.55\ d$ 2H.

*R(−)-2-Nitro-4-(3,2-chloropropionic acid butylester)-phenyl-4′-(10-undecenyloxy)-biphenyl-4-carboxylate (***IId***)*[20]. 2.5 mmol (0.92 g) of the acid VII and 2.5 mmol (0.76 g) of II were dissolved in 5 ml dry methylene chloride. Dimethylaminopyridine (DMAP) 6 mg was added and the mixture was cooled to 0°C. Dicyclohexanylcarbodiimide (DCC) 0.25 g in 5 ml of methylene chloride was added dropwise. After 3 h the temperature was raised to 20°C and stirring was continued for additionally 10 h. The mixture was filtered and the filtrate was evaporated to dryness. Recrystallization from ethanol gave 0.57 g product, yield 70%. $[\alpha]_D^{20} = -0.80°$ (chloroform). ^{1}H n.m.r.: $\delta = 0.92\ t$ 3H, $\delta = 1.2$–$1.5\ m$ 14H, $\delta = 1.64\ m$ 2H, $\delta = 1.80\ m$ 2H, $\delta = 2.02\ q$ 2H, $\delta = 3.28\ dd$ 1H, $\delta = 3.44\ dd$ 1H, $\delta = 3.98\ t$ 2H, $\delta = 4.17\ m$ 2H, $\delta = 4.46\ t$ 1H, $\delta = 4.94\ m$ 2H, $\delta = 5.80\ m$ 1H, $\delta = 6.98\ d$ 2H, $\delta = 7.34\ d$ 1H, $\delta = 7.57\ dd$ 3H, $\delta = 7.68\ d$ 2H, $\delta = 8.01\ d$ 1H, $\delta = 8.20\ d$ 2H.

The corresponding compounds **IIa**, **b**, **c**, and **e** were synthesized according to the same procedure.

*R(−)-2-Nitro-4-(3,2-chloropropionic acid methylester)-phenyl-4′-(10-undecenyloxy)-biphenyl-4-carboxylate (***IIa***).* $[\alpha]_D^{20} = -2.87°$ (chloroform). ^{1}H n.m.r.: $\delta = 1.2$–$1.5\ m$ 12H, $\delta = 1.80\ m$ 2H, $\delta = 2.02\ q$ 2H, $\delta = 3.28\ dd$ 1H, $\delta = 3.44\ dd$ 1H, $\delta = 3.80\ s$ 3H, $\delta = 3.98\ t$ 2H, $\delta = 4.46\ t$ 1H, $\delta = 4.94\ m$ 2H, $\delta = 5.80\ m$ 1H, $\delta = 6.98\ d$ 2H, $\delta = 7.34\ d$ 1H, $\delta = 7.57\ d+d$ 3H, $\delta = 7.68\ d$ 2H, $\delta = 8.01\ d$ 1H, $\delta = 8.20\ d$ 2H.

*R(−)-2-Nitro-4-(3,2-chloropropionic acid ethyl ester)-phenyl-4′-(10-undecenyloxy)-biphenyl-4-carboxylate (***IIb***).* $[\alpha]_D^{20} = -0.90°$ (chloroform). ^{1}H n.m.r.: $\delta = 1.26$–$1.6\ m$ 15H, $\delta = 1.81\ m$ 2H, $\delta = 2.04\ q$ 2H, $\delta = 3.30\ dd$ 1H, $\delta = 3.44\ dd$ 1H, $\delta = 4.05\ t$ 2H, $\delta = 4.23\ m$ 2H, $\delta = 4.44\ t$ 1H, $\delta = 4.96\ m$ 2H, $\delta = 5.81\ m$ 1H, $\delta = 7.00\ d$ 2H, $\delta = 7.36\ d$ 1H, $\delta = 7.57\ d+d$ 3H, $\delta = 7.71\ d$ 2H, $\delta = 8.04\ d$ 1H, $\delta = 8.22\ d$ 2H.

R(−)-2-Nitro-4-(3,2-chloropropionic acid propyl ester)-phenyl-4′-(10-undecenyloxy)-biphenyl-4-carboxylate

*(***IIc***).* $[\alpha]_D^{20} = -0.79°$ (chloroform). ^{1}H n.m.r.: $\delta = 0.92\,t$ 3H, $\delta = 1.2$–$1.55\,m$ 12H, $\delta = 1.68\,m$ 2H, $\delta = 1.80\,m$ 2H, $\delta = 2.02\,q$ 2H, $\delta = 3.28\,dd$ 1H, $\delta = 3.44\,dd$ 1H, $\delta = 4.0\,t$ 2H, $\delta = 4.17\,m$ 2H, $\delta = 4.48\,t$ 1H, $\delta = 4.94\,m$ 2H, $\delta = 5.80\,m$ 1H, $\delta = 6.98\,d$ 2H, $\delta = 7.34\,d$ 1H, $\delta = 7.57\,d{+}d$ 3H, $\delta = 7.68\,d$ 2H, $\delta = 8.01\,d$ 1H, $\delta = 8.20\,d$ 2H.

*R(−)-2-Nitro-4-(3,2-chloropropionic acid hexylester)-phenol-4′-(10-undecenyloxy)-biphenyl-4-carboxylate (***IIe***).* $[\alpha]_D^{20} = -0.44°$ (chloroform). ^{1}H n.m.r.: $\delta = 0.90\,t$ 3H, $\delta = 1.26$–$1.42\,m$ 16H, $\delta = 1.44\,m$ 2H, $\delta = 1.66\,m$ 2H, $\delta = 1.82\,m$ 2H, $\delta = 2.05\,q$ 2H, $\delta = 3.30\,dd$ 1H, $\delta = 3.46\,dd$ 1H, $\delta = 4.02\,t$ 2H, $\delta = 4.18\,m$ 2H, $\delta = 4.48\,t$ 1H, $\delta = 4.96\,m$ 2H, $\delta = 5.81\,m$ 1H, $\delta = 7.00\,d$ 2H, $\delta = 7.36\,d$ 1H, $\delta = 7.60\,d{+}d$ 3H, $\delta = 7.70\,d$ 2H, $\delta = 8.04\,d$ 1H, $\delta = 8.22\,d$ 2H.

Polymer **IIIe** *(Scheme 2).* Poly(dimethylsiloxane-*co*-hydrogenmethylsiloxane) (2.7/1) 0.25 g (0.96 mmol Si–H groups) and **IIe** 0.96 mmol (0.65 g) in a dry flask was dissolved in 10 ml of dry toluene. A catalyst, dicyclopentadienylplatinum(II)dicholoride 0.08 mg was added as 0.29 ml of a stock solution in toluene containing 2.8 mg/10 ml. The solution was bubbled with nitrogen and the flask was sealed with a septum. The reaction mixture was heated to 100°C for 24 h and a second addition of the same amount of catalyst was done. After additionally 24 h at 100°C the polymer in the solution was precipitated in methanol. The product was twice reprecipitated from chloroform into methanol. The purity of the polymer was checked with thin layer chromatography (t.l.c.) on silica gel with chloroform as eluent. No free side-chain could be detected. Finally, the polymer was dissolved in chloroform, filtered using a 0.2 μm micro filter, evaporated until dry and further dried in vacuum. Yield 0.69 g of off white polymer. ^{1}H n.m.r. ($CHCl_3$): $\delta = 0.0\,m$ 22H, $\delta = 0.5\,m$ 2H, $\delta = 0.88\,t$ 3H, $\delta = 1.2$–$1.5\,m$ 22H, $\delta = 1.64\,m$ 2H, $\delta = 1.79\,m$ 2H, $\delta = 3.25\,m$ 1H, $\delta = 3.46\,m$ 1H, $\delta = 3.96\,m$ 2H, $\delta = 4.17\,m$ 2H, $\delta = 4.46\,t$ 1H, $\delta = 4.68\,m$ 0.13H (remaining Si–H), $\delta = 6.98\,m$ 2H, $\delta = 7.34\,m$ 1H, $\delta = 7.56\,m$ 3H, $\delta = 7.66\,m$ 2H, $\delta = 8.02\,s$ 1H, $\delta = 8.18\,m$ 2H, all signals are broad.

The other polymers in this series were prepared in similar yields according to the same procedure.

Polymer **IIIa.** ^{1}H n.m.r.: $\delta = 0.0\,m$ 22H, $\delta = 0.5\,m$ 2H, $\delta = 1.2$–$1.6\,m$ 14H, $\delta = 1.79\,m$ 2H, $\delta = 3.25\,m$ 1H, $\delta = 3.46\,m$ 1H, $\delta = 3.78\,s$ 3H, $\delta = 3.96\,m$ 2H, $\delta = 4.46\,t$ 1H, $\delta = 4.68\,m$ 0.11H (remaining Si–H), $\delta = 6.98\,m$ 2H, $\delta = 7.34\,m$ 1H, $\delta = 7.56\,m$ 3H, $\delta = 7.66\,m$ 2H, $\delta = 8.02\,s$ 1H, $\delta = 8.18\,m$ 2H, all signals are broad.

Polymer **IIIb.** ^{1}H n.m.r.: $\delta = 0.0\,m$ 21H, $\delta = 0.5\,m$ 2H, $\delta = 1.2$–$1.5\,m$ 19H, $\delta = 1.79\,m$ 2H, $\delta = 3.28\,m$ 1H, $\delta = 3.46\,m$ 1H, $\delta = 3.96\,m$ 2H, $\delta = 4.24\,q$ 2H, $\delta = 4.46\,t$ 2H, $\delta = 4.68\,m$ 0.15H (remaining Si–H), $\delta = 6.98\,m$ 2H, $\delta = 7.34\,m$ 1H, $\delta = 7.56\,m$ 3H, $\delta = 7.66\,m$ 2H, $\delta = 8.02\,s$ 1H, $\delta = 8.18\,m$ 2H, all signals are broad.

Polymer **IIIc.** ^{1}H n.m.r.: $\delta = 0.0\,m$ 21H, $\delta = 0.5\,m$ 2H, $\delta = 0.93\,t$ 3H, $\delta = 1.2$–$1.5\,m$ 16H, $\delta = 1.64\,q$ 2H, $\delta = 1.79\,m$ 2H, $\delta = 3.28\,m$ 1H, $\delta = 3.46\,m$ 1H, $\delta = 3.96\,m$ 2H, $\delta = 4.14\,m$ 2H, $\delta = 4.49\,t$ 2H, $\delta = 4.7\,m$ 0.13H (remaining Si–H), $\delta = 6.98\,m$ 2H, $\delta = 7.34\,m$ 1H, $\delta = 7.56\,m$ 3H, $\delta = 7.66\,m$ 2H, $\delta = 8.02\,s$ 1H, $\delta = 8.18\,m$ 2H, all signals are broad.

Polymer **IIId.** ^{1}H n.m.r.: $\delta = 0.0\,m$ 19.4H, $\delta = 0.5\,m$ 2H, $\delta = 0.86\,t$ 3H, $\delta = 1.2$–$1.65\,m$ 20H, $\delta = 1.72\,m$ 2H, $\delta = 3.22\,m$ 1H, $\delta = 3.40\,m$ 1H, $\delta = 3.90\,m$ 2H, $\delta = 4.12\,m$ 2H, $\delta = 4.40\,t$ 2H, $\delta = 4.62\,m$ 0.11H (remaining Si–H), $\delta = 6.9\,m$ 2H, $\delta = 7.28\,m$ 1H, $\delta = 7.5\,m$ 3H, $\delta = 7.6\,m$ 2H, $\delta = 7.96\,s$ 1H, $\delta = 8.12\,m$ 2H, all signals are broad.

Polymer characterization

The polyhydrogenmethyldimethylsiloxanes used in this work had a hydrogenmethylsiloxane/dimethylsiloxane ratio of 1/2.7 and the degree of polymerization of about 30 according to the manufacturer. S.e.c. analysis in chloroform vs polystyrene standards gave a number average molar mass (M_n) of 1500 g mol^{-1} and a polydispersity index of 3.5. This gives a number average degree of polymerization (X_n) of 21. The polymer **IIIe** showed under the same conditions an M_n of 6900 g mol^{-1} with 3.1 in polydispersity index. This corresponds to $X_n = 28$.

The polymers do not show any glass transitions within the temperature interval studied. The phase transitions SmC*–SmA and SmA–I were clearly seen in d.s.c. experiments.

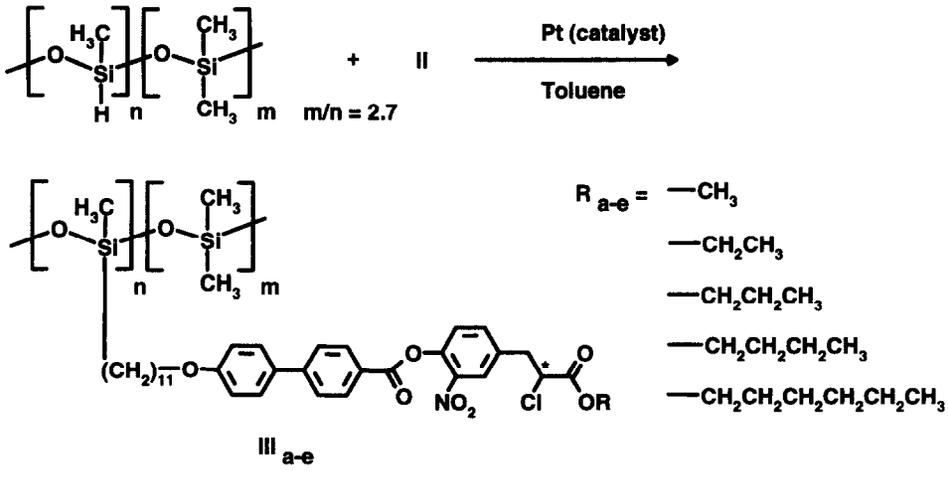

Scheme 2 Reaction to polymer

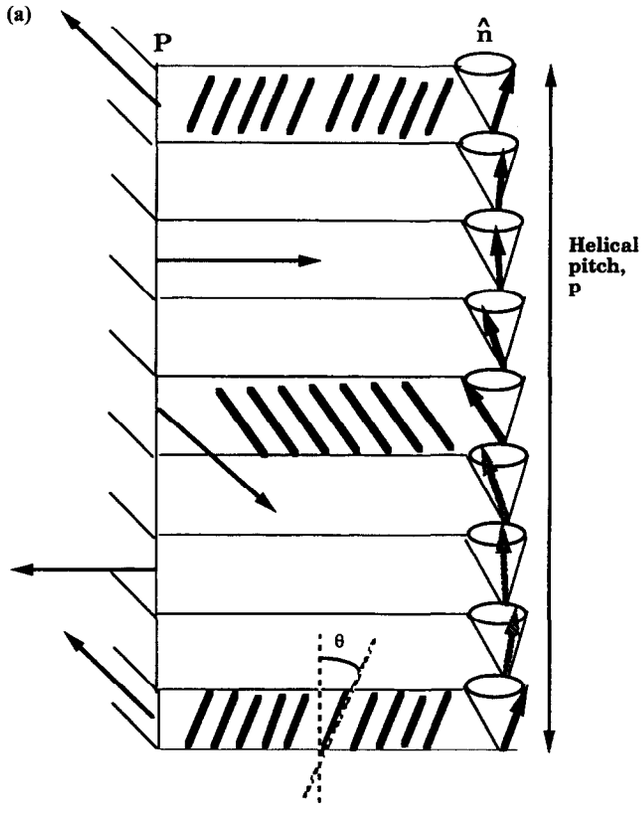

Figure 1 (a) Definition of tilt angle θ and direction of polarization vector P in a helicoidal smectic C* structure. (b) An un-wound chiral smectic structure

Phase transition temperatures °C

IIIa	S_C^* 88 S_A^* 140 Iso
IIIb	S_C^* 80 S_A^* 112 Iso
IIIc	S_C^* 87 S_A^* 119 Iso
IIId	S_C^* 70 S_A^* 104 Iso
IIIe	Cr 40 S_C^* 80 S_A^* 101 Iso

Determination of physical parameters

Ferroelectric polymerization and smectic tilt angles. The chiral smectic C phase offers a monoclinic environment which has a symmetry allowing polar order. The characteristic feature of the chiral smectic C phase is thus the existence of a macroscopic polarization P_S, which in low molar mass liquid crystals falls in the range $1-1000\,nC\,cm^{-2}$. The chirality induces a helical structure, which in an idealized case (*Figure 1a*) leads to polarization compensation. A polarized sample (*Figure 1b*), with a uniform polarization P in the sample, can be obtained by applying an external field, or by surface interactions. The polarization is temperature dependent, and approximately falls off with a power-law when approaching the paraelectric smectic A phase at higher temperature. The relation between the molecular dipoles and the resulting macroscopic values of P_S is not known in detail.

The measurement of the spontaneous polarization P_S can be done using a number of methods[21]: Using pyroelectric detection is a convenient method, also offering the advantage of not exposing the sample to strong d.c. fields, but on the other hand presents difficulties for absolute determination of P_S. Electrical measurements use either the bridge or the triangular wave method. The sample is switched between two polarization states $+P_S$ and $-P_S$, corresponding to tilt angles $+\theta$ and $-\theta$, by applying an external a.c. field strong enough to reach saturated polarization. Displaying the polarization current during the reversal, transformed to a voltage, as a function of applied voltage will produce a characteristic ferroelectric hysteresis loop on the storage oscilloscope screen. The amplitude of the loop U directly gives the spontaneous polarization[22] according to the formula

$$P_S = U/2AC$$

where A is the active area of the sample and C is the reference capacitor in the bridge. Alternatively, one can record and integrate the polarization reversal current when applying a triangular wave voltage. Results for P_S-values presented in this work come from the latter method. Measurements of the tilt angle are made with the d.c. method. This means that the sample is subjected to a d.c. electric field, and rotated between crossed polarizers in the microscope. Measuring the rotation angle between extinction positions with positive and negative polarity will give the smectic tilt angle. The tilt angle usually shows the same or nearly the same temperature dependence as the polarization

$$\theta \sim (T_c - T)^{\beta}$$

where the critical exponent β is 1/2 from the simplest thermodynamic model[21].

The electroclinic effect. In the orthogonal smectic A phase, where the side-chains are perpendicular to the

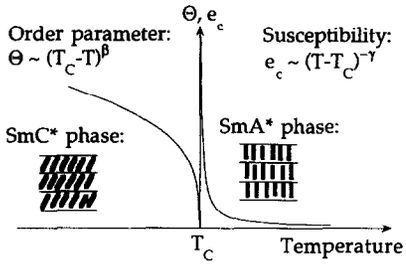

Figure 2 Qualitative temperature dependence of tilt angle and spontaneous polarization at the A–C* phase transition. Also shown is the diverging induced tilt angle in the A-phase

smectic layers, the electroclinic effect[23] manifests itself in a fast and linear electro-optic switching. The physical origin in the smectic A phase is the occurrence of the soft-mode, which leads to a diverging tilt angle near the A–C* transition temperature (cf. *Figure 2*). The electroclinic effect leads to a field-induced tilt angle, which transforms the A phase into a C* phase. For small applied electric fields and not too close to the A–C* transition, the induced tilt is linear in the field

$$\theta = e_c E$$

where e_c is the electroclinic coefficient given by

$$e_C = \mu/[\alpha(T - T_c)]$$

T_c being the temperature of the A–C* transition, α is the first constant in the Landau free-energy expression, and μ is the structural coefficient. *Figure 2* depicts the critical behaviour of the ferroelectric and electroclinic tilt angles. In the smectic A phase, the temperature dependence of e_C with $\gamma = 1$ represents the simplest thermodynamic model for the A–C* transition. One further characteristic of the electroclinic effect is the field independence of the response time, which is given by

$$\tau = \gamma_\theta/[\alpha(T - T_c)]$$

where γ_θ is the viscosity coefficient for the θ-motion. The value of the response times are in the 1–10 μs range for low-molar mass compounds. As can be seen from the last equation, there is a 'critical slowing down' near T_c close to the C*-phase, where the response time gets very long. At the same time the induced tilt angle θ becomes large. The behaviour is typically close to a paraelectric–ferroelectric phase transition (soft-mode excitation).

Measurements of the electroclinic tilt angles are made by the a.c. method[24]. This means that the sample is subjected to an alternating electric field, and the amplitude of the optical modulation is recorded. If the sample is oriented with the neutral, field-free optical axis at 22.5° to the polarizer, which is the setting with optimal sensitivity (*Figure 3*), the smectic tilt angle can be obtained from the observed optical modulation.

Sample preparation. The polymer samples are prepared for physical measurements in our specially designed shear cell[22]. For the electro-optic measurements of ferroelectric and electroclinic switching, the alignment geometry of *Figure 3* is preferable. Excellent alignment was obtained by shearing the sample in the smectic A phase close to the isotropic phase, and slowly cool it to the smectic C phase. The polymer sample was prepared between two ITO-coated glass plates that have been given a special electrode pattern by etching in order to have a well-defined overlapping area (16.8 mm^2) independent of shear position. In order to prevent electric breakthrough in the active area, a 1000 Å uniform SiO layer was deposited by normal incidence thermal evaporation, and patterned SiO-spacers define the cell thickness. The shear orientation cell is mounted in a Mettler FP52 hot stage for temperature control, and observed in Zeiss Photomicroscope equipped with a fast electro-optic recording system. The sample temperature is measured with a Pt100 resistor element close to the cell. As an alternative to the shear cells, standard commercial surface-coated cells with 4×4 mm^2 active area and 4 μm thickness can be used.

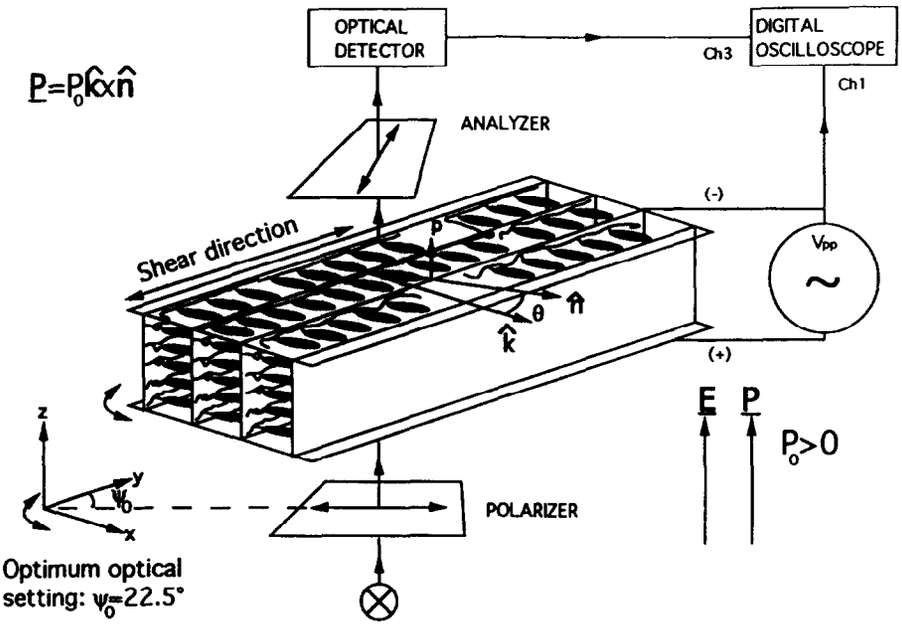

Figure 3 Sample geometry and experimental set-up

The cells can be capillary filled with the polymer in 6–8 h at 110–140°C, but generally produce poor alignment. One big advantage of the shear cells compared to the commercial cell is that they are filled much more rapidly, and provide better alignment.

RESULTS AND DISCUSSION

Synthesis and phase behaviour

For our system, tyrosine appeared to be an ideal choice of a precursor for the chiral group. The transformation of an α-amino acid into the corresponding α-chloro acid readily occurs via a diazotization in dilute hydrochloric acid. The reaction proceeds with inversion of the configuration at the reaction centre. However, in the tyrosine case this reaction was not feasible. Upon the treatment of tyrosine with sodium nitrite in dilute hydrochloric acid mostly tarry material was formed probably due to nitrosation of the aromatic ring. By introducing a nitro group in the aromatic ring the undesired reaction was suppressed and the diazotization reaction was readily performed. The different esters of the α-chloro acid were obtained by esterification using hydrogen chloride gas. The following esterification and the anchoring of the mesogenic side-chains to the siloxane copolymer using the hydrosilylation reaction proceeded as expected.

The aim of the physical measurements on polymers **IIIa–e** was to try to obtain correlations between phase behaviour (transition temperatures, ferroelectric and electroclinic properties), and the length of the side-chain. Phase designations were obtained by a combination of information from d.s.c. optical microscopy, and electro-optic behaviour. Results for the five members are shown in *Figure 4*. Compared to low-molecular FLCs, the study of polymeric FLCs presents some additional difficulties, especially in the interpretation of electro-optic response curves. A linear electro-optic response, characteristic of the electroclinic effect in the smectic A-phase, can often be found also in the tilted ferroelectric phases. The switching can be transformed into a regular ferroelectric switching by applying a strong enough electric field, but because of the polymeric state, the threshold fields are much larger than for low molecular weight liquid crystals. This effect is readily observed in a typical polymeric FLC (e.g. polymer **IIIe**), where a perfectly normal ferroelectric response is gradually transformed into a linear 'electro-clinic like' response at lower temperatures, where the higher viscosity and elasticity prevents the fully developed switching to be observed. This makes it difficult to ascertain the lower temperature limit for the ferroelectric C*-phase, and also to observe transitions to higher smectic phases, because response times of several seconds tend to smear out response characteristics. It is important to be aware of these polymer-specific characteristics when studying electric response phenomena and phase transitions in polymers. For these reasons, many phase designations in the literature on polymeric smectics have the form isotropic–smectic A–smectic C–smectic X. A full elucidation of the higher smectic phases requires extensive X-ray investigations on aligned samples. In this paper, we concentrate on the properties of the smectic A and C phases.

Physical properties

Characteristics of observed optical and current responses. The physical properties of the polymers addressed in this paper are the ferroelectric polarization, the smectic C tilt angle, and the electroclinic tilt angle, and the temperature behaviour of these parameters. In the measurements, the polymer sample is subjected to an electric excitation, and either the optical or the electrical response is monitored as a function of the applied signal. Let us illustrate some characteristic features of the response of the polymers to an electric a.c. signal by

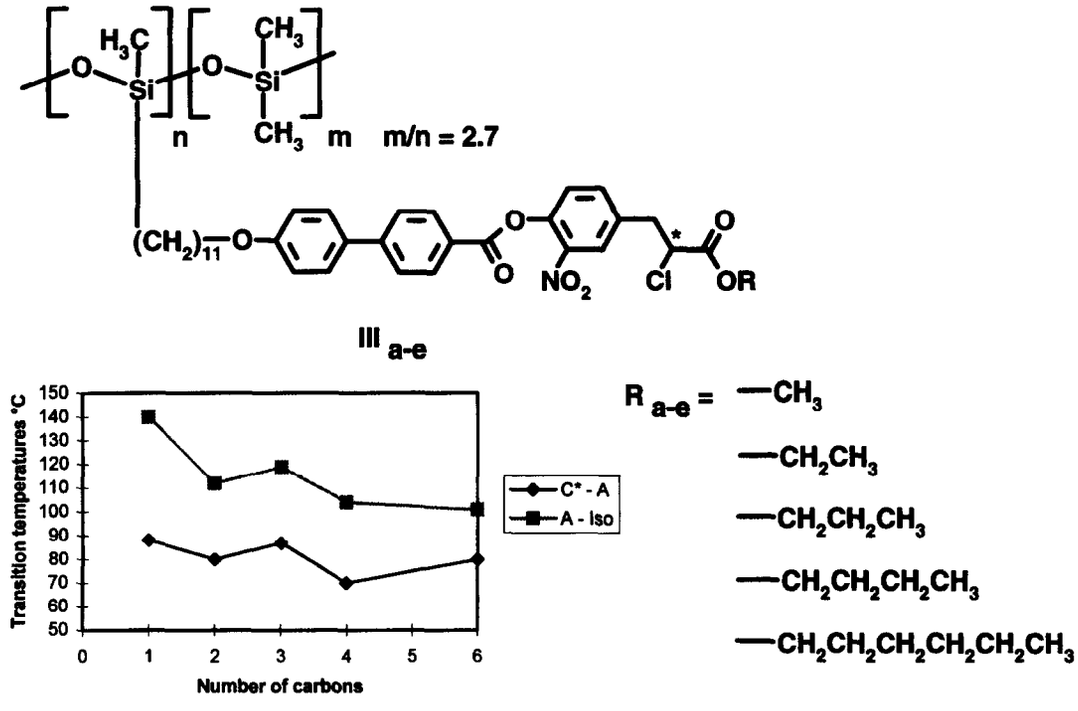

Figure 4 Phase behaviour of the five members studied in this work

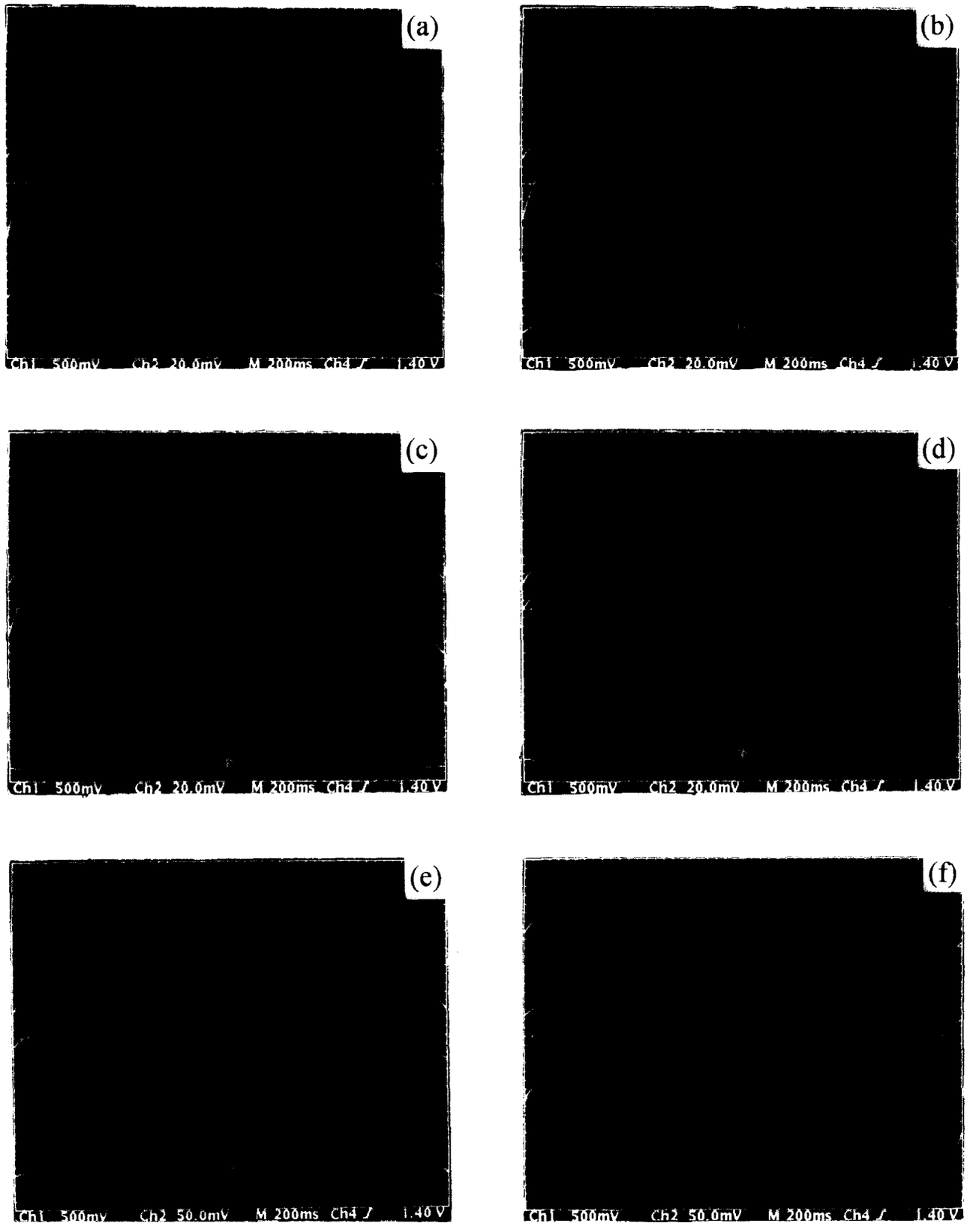

Figure 5 Typical electrical and optical responses (middle and bottom curves, respectively) in C* and A phases to an applied a.c. voltage (top curve). (a–e) Hexyl, (f) Propyl. (a) 86.3°C (A-phase). (b) 79.3°C (transition region A–C* phase). (c) 74.4°C (C*-phase). (d) 68.2°C (C*-phase). (e) 59.6°C (C*-phase). (f) 77.6°C (C*-phase). Applied voltage 150 V, frequency 1 Hz

giving a sequence of optical and polarization current recordings for the polymer with the longest side-chain (the hexyl member). The excitation is a triangular wave of 75 V amplitude and 1.0 Hz frequency. In the smectic A phase, the typical linear electroclinic response is found, as illustrated with the recording at 86.3°C (*Figure 5a*). The cell conduction is rather high, which gives a large background current following the driving voltage. At 79.3°C (*Figure 5b*) the linear optical response is rounded, as the response has features of both electroclinic and ferroelectric switching, typical of a low molecular weight FLC in the transition region between smectic A and C*

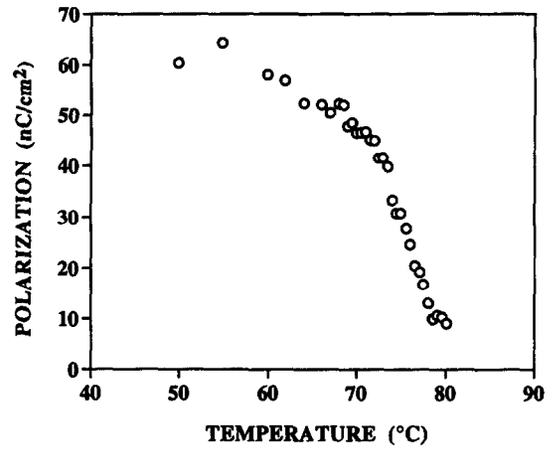

Figure 6 Polarization vs temperature for the hexyl member

phases. The background current has diminished somewhat. At 74.4°C *(Figure 5c)*, the ferroelectric cone switching is fully developed, with the optic axis reaching its extreme directions every half-cycle. The background current has further diminished, and the polarization reversal current peak, occurring simultaneously as the optical switching, is becoming more pronounced. At 68.2°C (*Figure 5d*), there is a slight change in the shape of the optical response, due to the fact that the optic axis rotates more than 45° upon field reversal, which between crossed polarizers gives a small maximum in the transmitted intensity immediately after field reversal. The current peak is still more pronounced, due to the decrease of the conductivity of the sample, and the increase of the spontaneous polarization of the cell. At lower temperatures (59.6°C) (*Figure 5e*) the increased rotational viscosity makes the response times too long for the switching to be fully developed. Moreover, the polarization current will be smeared out and no longer visible as a distinct peak in the current response.

As a comparison, *Figure 5f* shows the responses for the polymer with side-chain with propyl terminal group, **IIIc**. In the smectic A phase, the response is similar to polymer **IIIe**, but in the smectic C* phase there is no sign of a polarization current peak. Trying different waveforms in the driving voltage, or altering the frequency and amplitude, does not change the situation markedly. Since it was not possible to detect the reversal current for this polymer, and also not for polymer **IIIb**, these two polymers could not be included in the comparison of how polarization depends on side-chain length.

Spontaneous polarization and tilt angle data. The measured curve for the spontaneous polarization for **IIIe** shows a deviation at the smectic C*-smectic A transition from the simple power-law behaviour, with a steep decrease of P_S near T_c. In *Figure 6* is shown the measured polarization curve for **IIIe**. It saturates at about 55 nC cm^{-2}. The saturated values for **IIIa** and **IIId** were found to be 60 and 130 nC cm^{-2}, respectively.

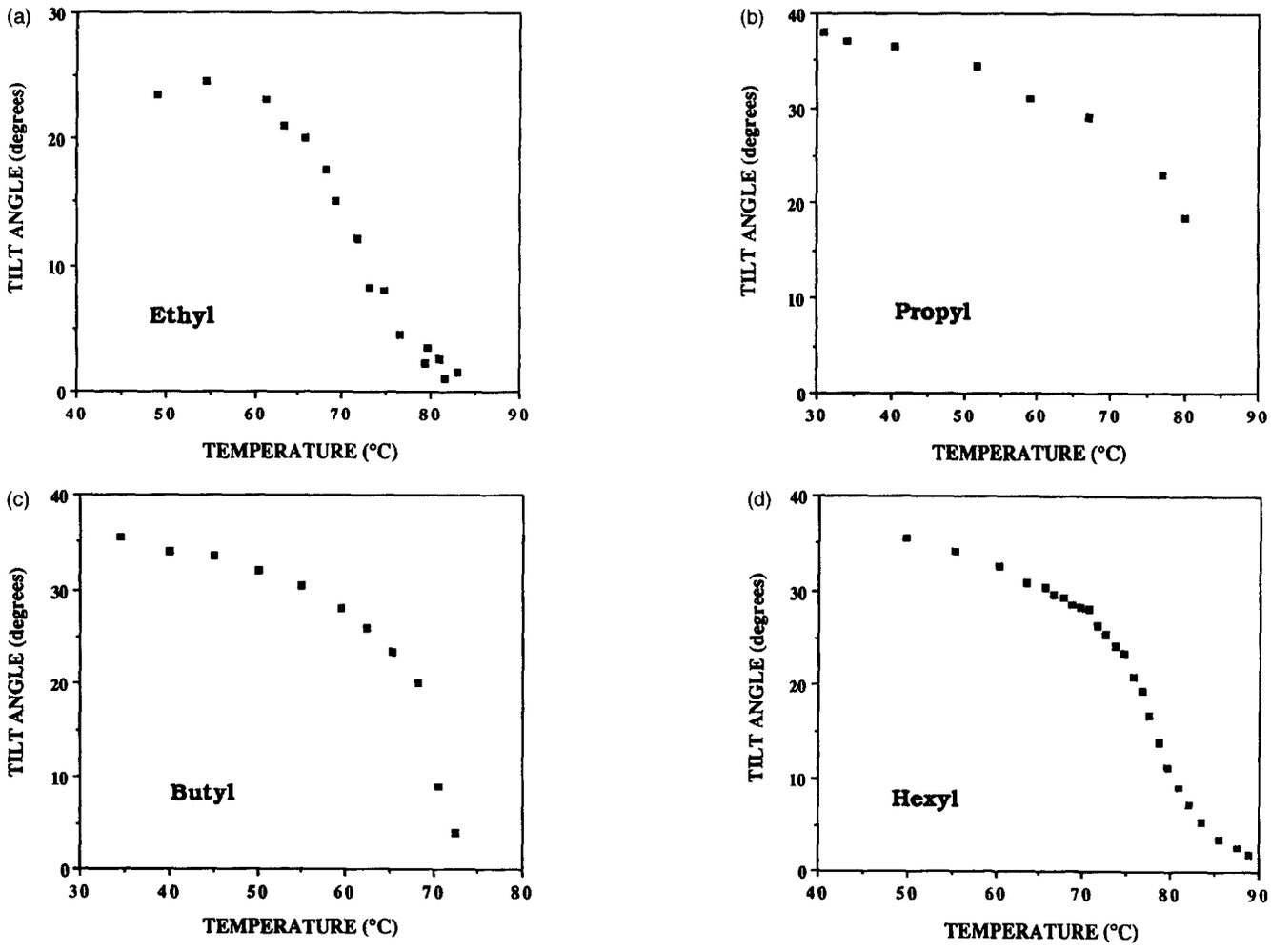

Figure 7 Measured tilt angles in the ferroelectric C*-phase for four members in the series. (a) Ethyl. (b) Propyl. (c) Butyl. (d) Hexyl

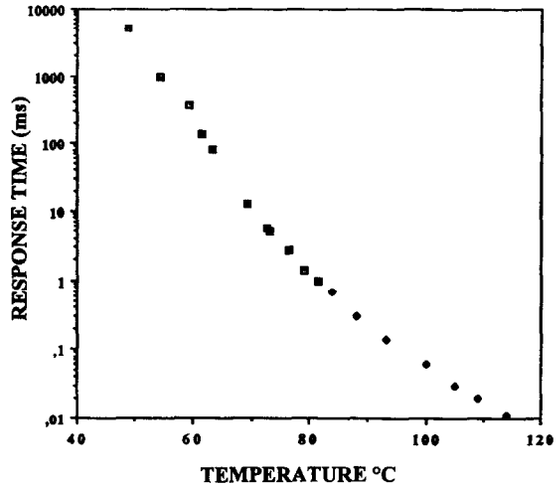

Figure 8 Electro-optic response time vs temperature for the ethyl member in the C*- and A-phases

These data suggest that there might be a most favourable configuration for high polarization at intermediate chain lengths.

Tilt angles for four members of the series are shown in *Figure 7*. Tilt angles in the C*-phase were measured for the ethyl, propyl, butyl and hexyl members. Values at $T_c - T = 30$ K were found to be 23°, 34°, 33° and 35°, respectively.

An example of measurement of electro-optic response times as a function of temperature for the ethyl member is shown in *Figure 8*. There is a continuous, approximately exponential decrease in the response time when going from the deep C*-phase into the A-phase. The switching times range from several seconds down to about 10 μs near the isotropic transition.

Electric field response at the smectic C–A transition.* The linear characteristic in the tilt-field graph is gradually transformed into a constant tilt angle when entering the smectic C* phase. A good example is given in *Figure 9*, where the induced tilt angle as a function of applied voltage for the propyl member is plotted for different temperatures. The strictly linear curve from the pure electroclinic response is gradually changed into a nearly field-independent curve, coming from the fact that the tilt angle in the smectic C* phase is unaffected by the field, except very close to the transition. The slight field-dependence at low fields is probably due to reorientations of a biased director alignment before the measuring field is applied.

Induced tilt angles as a function of applied field is shown in *Figure 10* for four members at a temperature 4 K above the smectic C*–A transition. A remarkably regular dependence is found for the electroclinic coefficient (the slope of the straight line) as a function of the side-chain length: the coefficient increases with side-chain length.

The frequency response of the electroclinic effect gives information on how well the electroclinic response is described by a single-frequency soft-mode model. This model means that the electroclinic optical response is modelled exactly as the dielectric response, with a single-frequency Debye model[21]. Usually the electroclinic relaxation frequency correlates with the relaxation frequency found from the dielectric response. In

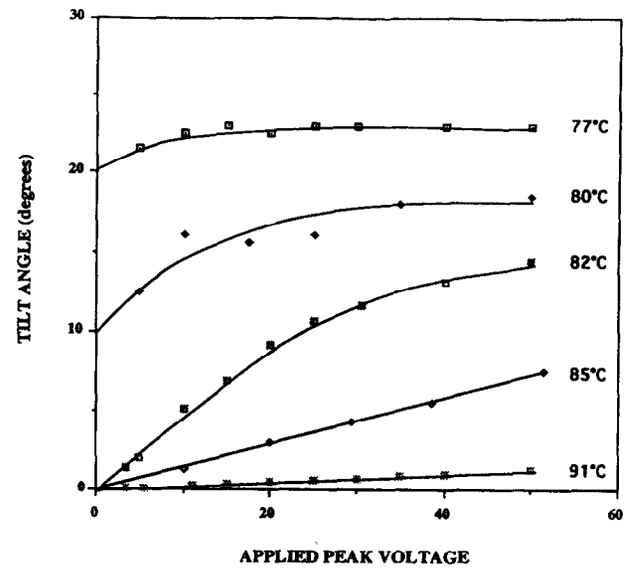

Figure 9 Induced tilt angle as a function of applied voltage for the propyl member. The linear characteristic is gradually transformed into a constant tilt angle when entering the smectic C* phase

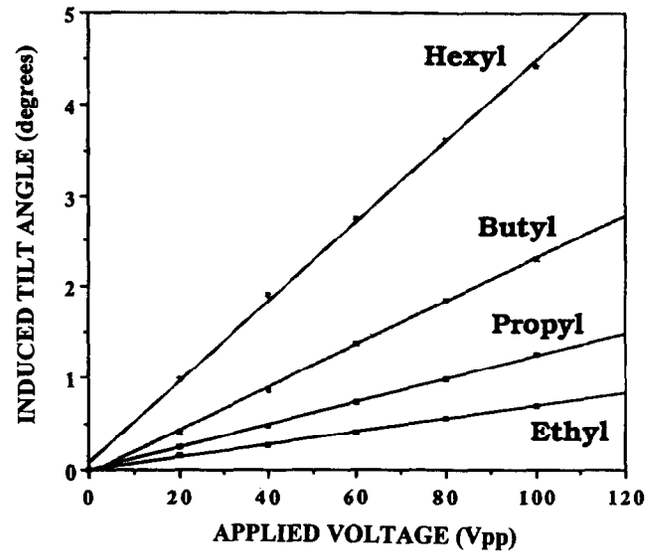

Figure 10 Comparison of electroclinic tilt angles as a function of applied voltage for four members of the series. All data recorded 4 K above the smectic C*–A transition

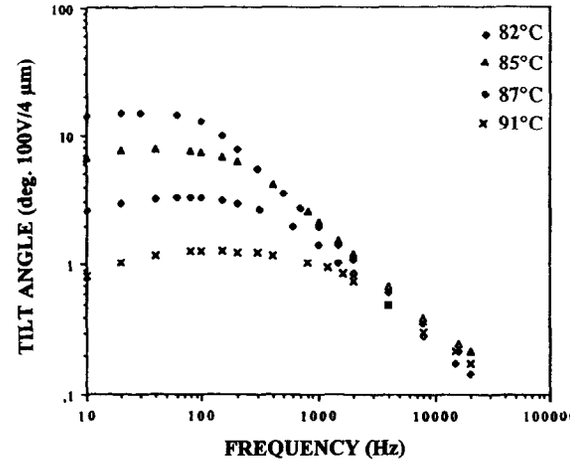

Figure 11 Frequency response curves for the propyl member in the smectic A-phase

Figure 11 we show the results for the propyl member at four different temperatures. The value for the exponent at high frequencies is close to the Debye model value −1. The optical response time at $T - T_c = 7$ K for the hexyl is 0.6 ms, and for the butyl 0.35 ms. For the hexyl, propyl and methyl the relaxation frequencies were found to be 620, 410 and 270 Hz, respectively.

CONCLUSIONS

The synthesis of a series of side-chain polymers differing only in side-chain length was demonstrated. The chiral mesogen is derived from tyrosine. All five members exhibit liquid crystalline phases of types smectic A and C*. The spontaneous polarization in the ferroelectric phases of three of the members could be measured, and was found to be in the 55–130 nC cm^{-2} range. The dynamics of the electroclinic response in the orthogonal A phase was studied, and a correlation between side-chain length and electroclinic relaxation time was found. The influence of the mesogen length on smectic layer spacing have recently been investigated by X-ray scattering on thick films. Preliminary results show an unexpected reverse dependence of layer spacing on mesogen length[25].

ACKNOWLEDGEMENTS

Financial support from The Swedish Natural Science Research Council and The Swedish Technical Science Research Council is gratefully acknowledged.

REFERENCES

1. Meyer, R. B., Liebert, L., Strzelecki, L. and Keller, P., *J. Phys. (Paris) Lett.*, 1975, **36**, 69.
2. Shibaev, V. P., Kozlowskii, M. V., Beresnev, L. A., Blinov, L. M. and Platé, N. A., *Polym. Bull.*, 1984, **12**, 299.
3. Uchida, S., Morita, K., Miyoshi, K., Hashimoto, K. and Kawasaki, K., *Mol. Cryst. Liq. Cryst.*, 1988, **155**, 93.
4. Scherowsky, G., Schliwa, A., Springer, J., Kuenpast, K. and Trapp, W., *Liq. Crystals*, 1989, **5**, 1281.
5. Bömelburg, J., Heppke, G. and Hollidt, J., *Makromol. Chem., Rapid Commun.*, 1991, **12**, 483.
6. Skarp, K., Andersson, G., Lagerwall, S. T., Kapitza, H., Poths, H. and Zentel, R., *Ferroelectrics*, 1991, **122**, 127.
7. Skarp, K., Andersson, A., Zentel, R. and Poths, H., *Proc. SPIE* 1995, **2408**, 32.
8. Kocot, A., Wrzalik, R., Vij, J. K. and Zentel, R., *J. Appl. Phys.*, 1994, **75**, 728.
9. Brehmer, M., Zentel, R., Wagenblast, G. and Siemensmeyer, K., *Macromol. Chem. Phys.*, 1994, **195**, 1891.
10. Vallerien, S. U., Kremer, F., Fischer, E. W., Kapitza, H., Zentel, R. and Poths, H., *Makromol. Chem, Rapid Commun.*, 1990, **11**, 593.
11. Ozaki, M., Utsumi, M., Yoshino, K. and Skarp, K., *Jpn. J. Appl. Phys.*, 1993, **32**, L852.
12. Küpfer, J. and Finkelmann, H., *Makromol. Chem. Rapid Commun.*, 1991, **12**, 717.
13. Finkelmann, H., in *Thermotropic Liquid Crystals*, ed. G. W. Gray. Wiley, 1987.
14. Zentel, R., in *Liquid Crystals*, ed. H. Stegemeyer. Steinkopff Verlag, Darmstadt, 1994.
15. Svensson, M., Helgee, B., Hjertberg, T., Hermann, D. and Skarp, K., *Polym. Bull.*, 1993, **31**, 167.
16. Ozaki, M., Sakuta, M., Yoshino, K., Helgee, B., Svensson, M. and Skarp, K., *Appl. Phys.*, 1994, **B59**, 601.
17. Johnson, T. B. and Kohmann, E. F., *J. Am. Chem. Soc.*, 1915, **37**, 1863.
18. Fu, S.-C. J., Birnbaum, S. M. and Greenstein, J. P., *J. Am. Chem. Soc.*, 1954, **76**, 6054.
19. Percec, V., Zheng, Q. and Lee, M., *J. Mater. Chem.*, 1991, **1**, 611.
20. Neises, B. and Steglich, W., *Angew. Chem.*, 1978, **90**, 556.
21. Skarp, K. and Handschy, M., *Mol. Cryst. Liq. Cryst.*, 1988, **165**, 439.
22. Skarp, K. and Andersson, G., *Ferroelectrics*, 1986, **6**, 67.
23. Garoff, S. and Meyer, R. B., *Phys. Rev. Lett.*, 1977, **38**, 848.
24. Andersson, G., Dahl, I., Keller, P., Kuczynski, W., Lagerwall, S. T., Skarp, K. and Stebler, B., *Appl. Phys. Lett.*, 1987, **51**, 640.
25. Skarp, K., Svensson, M., Helgee, B., Ozaki, M. and Yoshino, K. (to be published).